HHS Public Access

Author manuscript

*Biotechnol Appl Biochem*. Author manuscript; available in PMC 2017 January 04.

Published in final edited form as:

*Biotechnol Appl Biochem*. 2016 ; 63(1): 113–124. doi:10.1002/bab.1344.

# Antiproliferative effects of ZnO, ZnO-MTCP, and ZnO-CuMTCP nanoparticles with safe intensity UV and X-ray irradiation

**Susan Sadjadpour**[1], **Shahrokh Safarian**[1,*], **Seyed Jalal Zargar**[1], and **Nader Sheibani**[2]

[1]School of Biology, College of Science, University of Tehran, Tehran, Iran

[2]Departments of Ophthalmology and Visual Sciences, and Biomedical Engineering, University of Wisconsin School of Medicine and Public Health, Madison, WI, USA

## Abstract

In photodynamic therapy (PDT) of cancer both the light and the photosensitizing agent are normally harmless, but in combination they could result in selective tumor killing. Zinc oxide nanoparticles were synthesized and coated with the amino acid cysteine to provide an adequate arm for conjugation with porphyrin photosensitizers (meso-tetra (4-carboxyphenyl) porphyrin [MTCP] and CuMTCP). Porphyrin-conjugated nanoparticles were characterized by TEM, FTIR, and UV–vis, and fluorescence spectrophotometry. The 3-[4, 5-dimethylthiazol-2-yl]-2,5-diphenyl tetrazolium bromide (MTT) assay was used to measure cell viability in the presence or absence of porphyrin conjugates following UV and X-ray irradiation. The uptake of the porphyrin-conjugated ZnO nanoparticles by cells was detected using fluorescence microscopy. Our results indicated that the survival of T-47D cells was significantly compromised in the presence of ZnO-MTCP-conjugated nanostructures with UV light exposure. Exhibition of cytotoxic activity of ZnO-MTCP for human prostate cancer (Du145) cells occurred at a higher concentration, indicating the more resistant nature of these tumor cells. ZnO-CuMTCP showed milder cytotoxic effects in human breast cancer (T-47D) and no cytotoxic effects in Du145 with UV light exposure, consistent with its lower cytotoxic potency as well as cellular uptake. Surprisingly, none of the ZnO-porphyrin conjugates exhibited cytotoxic effects with X-ray irradiation, whereas ZnO alone exerted cytotoxicity. Thus, ZnO and ZnO-porphyrin nanoparticles with UV or X-ray irradiation may provide a suitable treatment option for various cancers.

### Keywords

ZnO nanoparticles; MTCP; SLPDT; T-47D; Du145

## 1. Introduction

The incidence of cancer, in parallel with industrial development, has been increasing and threatens more lives [1]. Cancer nanotechnology is an interdisciplinary field of science incorporating nanotechnology, biotechnology, and medicine to design nanoengineered particles as multifunctional diagnostic and therapeutic systems. These are developed to reach

*Address for correspondence: Shahrokh Safarian, Associate Professor of Biochemistry, School of Biology, College of Science, University of Tehran, 14176-14411, Tehran Iran, Tel.: +9821-61113312, Fax: +9821-66405141. safarian@khayam.ut.ac.ir.

specific molecular targets in diseased cells [2, 3]. The nanoparticles with broad medical applications are involved in molecular imaging, molecular diagnosis, and targeted therapy [4]. A large number of nanodrugs have now been produced by pharmaceutical industry, which provide profound beneficial effects in destroying cancerous cells with minimum side effects on normal cells [3].

Nanometer size particles have unique properties that are not comparable with larger size materials [5]. Nanoparticles have large surface areas for attachment of the functional groups constructing adequate stands for multiple diagnostic and antiproliferative therapeutic agents [3]. Zinc oxide (ZnO) nanoparticles are water-soluble semiconductor materials with a wide band gap. They have attracted interest because of their size-dependent optical and electrical properties [6]. In addition, ZnO nanoparticles, due to their luminescence properties, have potential applications with X-ray or ultraviolet light radiation provided by low voltage [1]. ZnO nanoparticles are being considered in numerous strategies for preparing the next generation of drugs including antimicrobial, bioimaging probes, and antiproliferative agents [1, 7].

There are some reports indicating the existence of cytotoxic effects with the use of metal-based nanoparticles [8–14]. Metal oxides such as zinc oxide or titanium dioxide commonly exert their cytotoxic effects via oxidative stress and DNA damage, resulting in autophagy and/or apoptosis [13, 14]. Thus, when the main goal is to construct a metal-based antiproliferative nanosystem, consisting of two or more functional moieties, part of the expected cytotoxicity may be attributed to the metal moiety, and the remaining part to the other cytotoxic functional group(s). However, when cells are treated with a nanosystem it may be possible that they feel the nontoxic concentration of the nanoparticle moiety but respond to the toxic concentrations of the bound functional group(s). Thus, the exhibited cytotoxicity to such a nanosystem should be totally attributed to the functional group(s). In this state, a nanoparticle could work only as a neutral carrier to facilitate cellular penetration of the nanosystem [11–14].

Photodynamic therapy (PDT) is a clinical treatment method for many diseases including various types of solid tumors [15]. The important basic concept of PDT is the combination of two therapeutic factors, the photosensitizer and light. Both factors are harmless alone, but when combined they become tumor destructive. Chen and Zhang created a new modality of PDT, self-lighting photodynamic therapy (SLPDT), in which the combination of radiotherapy and PDT provides a less expensive and more efficient treatment for cancer [1]. In this method of treatment, the photosensitizer links to the water-soluble nanoparticle and becomes sensitive to an appropriate wavelength, producing free radicals to kill the cancer cells under irradiation [16]. During radiotherapy, when the nanoparticles are irradiated, the particles generate visible light to excite the photosensitizer causing production of singlet oxygen and reactive oxygen species (ROS), the main mediator of cellular death in self-lighting PDT. In deep tumor treatments, X ray can be used as a good penetrating radiation to excite the nanoparticles for stimulation of the linked photosensitizer to produce ROS for cell killing [15, 17].

ZnO-based nanoparticles are one of the best choices for self-lighting PDT due to its effective near-band-edge emission in the UV region, which matches well with the UV absorption area of the most porphyrin photosensitizers. Moreover, ZnO nanoparticles have proper ability alone to become excited with light and acting as the photosensitizers to produce ROS for cell killing [17–19]. In fact, semiconducting properties of ZnO nanoparticles are responsible for production of ROS and cell death, even if antioxidative capacity of the cells is increased [1, 19]. ZnO nanoparticles have antiproliferative effects in millimolar concentrations [20, 21].

Efficiency of PDT largely relates to the amount of the produced singlet oxygen or free radicals, which is dependent on the photosensitizers' efficacy, light characteristics (e.g., intensity and wavelength), and oxygen concentration in the environment [1]. Here we focused on the antiproliferative effects of ZnO-porphyrin nanoparticles in Du145 prostate and T-47D breast cancer cells under safe intensity of UV and X-ray irradiation. We found that our constructed ZnO and ZnO-porphyrin nanosystems (especially ZnO-MTCP; zinc oxide-MTCP [meso-tetra(4-carboxyphenyl) porphyrin]) had notable potency to kill breast and prostate cancer cells.

## 2. Materials and Methods

### 2.1. Materials

Diethylene glycol, zinc acetate dihydrated, and L-cysteine (nonanimal) were purchased from Sigma-Aldrich (St. Louis, MO, USA), and were used to synthesize the water-soluble zinc oxide nanoparticles. MTCP and its copper containing derivative (CuMTCP), as the optically active material, were obtained from Frontier Scientific (Logan, UT, USA). These porphyrin compounds were conjugated to cysteine-coated ZnO nanoparticles to synthesize self-lighting antiproliferative drugs. 1-Ethyl-3-(3-dimethylaminopropyl)carbodiimide (EDC) and *N*-hydroxysulfosuccinimide (sulfo-NHS) were obtained from Sigma-Aldrich and were used for chemical conjugation of MTCP or CuMTCP to cysteine-coated ZnO nanoparticles. Roswell Park Memorial Institute Medium 1640 (RPMI) and fetal bovine serum (FBS) were purchased from Invitrogen (Carlsbad, CA, USA). The 3-[4,5-dimethylthiazol-2-yl]-2,5-diphenyl tetrazolium bromide (MTT), penicillin-streptomycin solution, and dimethyl sulfoxide (DMSO) were obtained from Sigma-Aldrich. Econo-Pac 10DG desalting columns were obtained from BioRad (Hercules, PA, USA).

### 2.2. Methods

**2.2.1. Preparation of zinc oxide nanoparticles—**Preparation of ZnO nanoparticles was carried out using the previously reported sol–gel method with some modifications [22]. Sol–gel is a simple and suitable method for production of nanoparticles having ordered crystal structures containing particles with narrow dispersed-size distribution [17, 22]. Synthesizing 10 mL colloidal zinc oxide nanoparticles was performed in a round-bottom flask using 0.0108 g zinc acetate. The diethylene glycol (10 mL) was then added to flask and refluxed for 40 Min with vigorous stirring at 110 °C. The temperature was then increased to 160 °C and subsequently kept under constant temperature for 30 Min until ZnO nanoparticles (5 mM) were made. Molar concentrations of ZnO and its porphyrin-conjugated forms were estimated based on previous reports [16, 17]. After the solution

cooled to room temperature, the pH was adjusted to 7.0. The coating of the ZnO nanoparticles was carried out by the addition of 0.1 mL of L-cysteine solution (0.5 M) and stirring for 48 H at 60 °C. The pH of the resulting solution was then adjusted to 7.0. The ZnO nanoparticles were purified using Econo-Pac 10DG desalting columns with the cutoff molecular size of 6,000 Da.

**2.2.2. Bioconjugation of ZnO nanoparticles with MTCP or CuMTCP—** Conjugation of MTCP or CuMTCP to ZnO nanoparticles was carried out by adding EDC ($5 \times 10^{-5}$ mol) and sulfo-NHS ($5 \times 10^{-5}$ mol) to 0.5 mL of MTCP (1.25 mM) or CuMTCP (1.25 mM) at room temperature in the dark. After 15 Min, the solution was added to 1 mL of ZnO (5 mM) and kept at room temperature in the dark for 2 H. The pH of the resulted solution was then adjusted to 7.0 and purified through Econo-Pac 10DG desalting columns.

**2.2.3. Characterization of cysteine-coated and MTCP-conjugated ZnO nanoparticles—**The size identification of the synthesized ZnO nanoparticles was determined using a transmission electron microscope (100 kV; LEO 906-Germany). For this purpose, the nanoparticles were sonicated for approximately 4 Min and loaded on the carbon-coated copper grid (mesh 200) and allowed to air dry. Spectrophotometric characteristics of ZnO nanoparticles were determined using luminescence as well as UV–vis spectrophotometery (Perkin Elmer, Australia). The determination of the free and chemical groups on the surface of the synthesized nanoparticles was performed by Fourier transform infrared (FTIR) spectroscopic analysis in the range of 500–4,000 $cm^{-1}$ using a spectrophotometer (Shimadzo, Tokyo, Japan). FTIR spectra of the free and conjugated MTCP were obtained for each related powder form prepared by centrifugation twice at 13,000×$g$ for 10 Min each and allowed the pellet to dry.

**2.2.4. Cell culture—**Human prostate cancer (Du145) and human breast cancer (T-47D) cell lines were obtained from National Cell Bank of Iran with the ATCC number HTB-81 and HTB-133, respectively. Cells were cultured in RPMI-1640 supplemented with 10% FBS and 1% penicillin-streptomycin. Cells were incubated at 37 °C, under 5% $CO_2$ and humidified condition. The passage number for T-47D and Du145 cell lines was 3 and 5, respectively.

**2.2.5. Cytotoxicity assay—**For cytotoxicity assay, $10^4$ cells/well were seeded in enzyme-linked immunosorbant assay (ELISA) microtiter plates. After 24 H, different concentrations of the cysteine-coated and porphyrin-conjugated forms of ZnO nanoparticles were added to the wells, and their cytotoxic effects were determined after 48 and 72 H. The cytotoxicity of the free MTCP or CuMTCP at the three concentrations 0.75, 1.5, and 7.5 μM was evaluated. The concentrations for ZnO-porphyrins in the cytotoxicity test were 10, 30, and 60 μM. Molar concentrations of ZnO and its porphyrin-conjugated forms were estimated based on previous reports [16, 17]. Cytotoxicity under the treatment was determined using the MTT assay based on the activity of mitochondrial succinate dehydrogenase in the live cells [23]. Following incubation, the culture medium was removed and cells were washed with PBS and incubated with the MTT solution (0.5 mg/mL in PBS) for 4 H. DMSO (100 μL in each well) was then added to dissolve the produced formazan crystals in the wells. The optical

density was measured using a microplate reader (RT-2100 C; Rayto, Shenzhen, People's Republic of China) at 570 nm. Optical absorptions of the treated samples were compared with those of the untreated cells to obtain percentage values for live cells. Cytotoxicity of the uncoated form of ZnO nanoparticles was not considered, since uncoated ZnO nanoparticles were not stable enough to give an adequate suspension. Therefore, only cysteine-coated ZnO nanoparticles were used. Our preliminary evaluations indicated that different forms of the cysteine-coated ZnO nanoparticles (ZnO-Cys), as well as its porphyrin-conjugated forms (ZnO-MTCP or ZnO-CuMTCP), did not have any cytotoxic effects in the dark as previously reported for ZnO nanoparticles [24].

**2.2.6. Photo killing—**For photo killing experiments, $l0^4$ cells were seeded in each well of a 96-well microtiter plate and incubated for 24 H at 37 °C and 5% $CO_2$ in the dark. The cells were then incubated with different concentrations of cysteine-coated and porphyrin-conjugated forms of ZnO nanoparticles (10, 30, and 60 μM) and incubated for an additional 48 H under similar conditions. Following incubation, the culture medium was changed and cells were exposed to UV-A/B (100 $\mu W/cm^2$) for 180 Sec and followed by an additional 24 H of incubation in the dark. The amount of energy and the time of UV irradiation were selected to have no cytotoxic effects on the cells. The similar intensity and duration of UV irradiation are also used by others [18]. For X-ray irradiation, cells were incubated with the same concentrations of ZnO-porphyrin conjugates as described above and then were exposed to X-ray (0.94 Gy) for 30 Sec under dental radiology X-ray apparatus (Costruzioni Elettroniche Industriali Automatismi (CEIA), Arezzo, Italy). X ray irradiation of the cells was provided using 12 shots of dental radiology apparatus (2.5 Sec each) under 70 kV and 8 mA.

**2.2.7. Fluorescence imaging—**Cellular uptake of nanoparticles was monitored by fluorescence microscopy (Zeiss Axioplan 2 imaging; Göttingen, Germany). Before microscopic examination, Du145 and T-47D cells were seeded on poly-L-lysine-coated coverslips placed in six-well plates and incubated for 24 H at 37 °C in the dark. Cells were then incubated with 60 μM of ZnO-MTCP nanoparticles for 24 H under same conditions. Culture medium was removed, and coverslips were washed twice with PBS. Cells were fixed with paraformaldehyde (4% in PBS) and washed with PBS. Following fixation, cells were incubated with fresh sodium borohydride (10 mg/mL) for 20 Min to eliminate autofluorescence. After incubation, cells were washed three times with Tris buffer saline (TBS: 20 mM Tris–HCl, 150 mM NaCl, pH 7.5) and coverslips were mounted on glass slides for fluorescence imaging.

**2.2.8. Statistical analysis—**The *t*-test statistical analysis was utilized in all experiments using SPSS and Excel software. The *P* value of less than 0.05 was considered statistically significant.

## 3. Results and Discussion

ZnO nanoparticles were synthesized based on the gel–sol reaction. The synthesized nanoparticles were coated with L-cysteine to prevent their aggregation tendency and placing adequate arms on the nanoparticles for porphyrin conjugation as previously described [25].

Coating of ZnO nanoparticles with L-cysteine occurred through a chemical bond between the SH group and zinc ion. The surface of the cysteine-coated nanoparticles containing the –$NH_2$ chemical group has a tendency to chemically react with the –COOH group of porphyrins (MTCP or CuMTCP), when the latter group becomes activated by EDC and Sulfo-NHS [17, 26]. Porphyrin derivatives were utilized to react with ZnO nanoparticles because their absorption characteristics are in good accordance with the emission properties of ZnO. Thus, fluorescence resonance energy transfer (FRET) between ZnO and porphyrin moiety could occur. Scheme 1 depicts conjugated form of ZnO nanoparticles when the amide bonds between the –$NH_2$ groups of the cysteines and –COOH groups of MTCP are formed. TEM images of ZnO nanoparticles are shown in Figs. 1a and 1b. These figures present spherical and hexagonal structures of the nanoparticles with the approximate size of 3–26 nm. None of the other irregular morphologies such as the rod-shaped particles were detected.

UV–vis absorption spectra of ZnO and its cysteine-coated structure are shown in inset of Fig. 2. The maximum absorbance of both samples was placed around 250 nm. However, the absorption intensity of ZnO-Cys nanoparticles was greater than ZnO and shifted about 5 nm to a lower wavelength. This occurred because of the smaller size of ZnO-Cys nanoparticles and conversion of these particles into better quantum dots having higher absorbance at the lower wavelength of 245 nm. The absorbance of the cysteine molecules was also recorded. The lack of absorbance at 250 nm indicated that the increased absorption intensity for ZnO-Cys nanoparticles was not because of the bound cysteines (not shown) [27, 28].

Fluorescence spectra of ZnO, ZnO-Cys, ZnO-MTCP, and ZnO-CuMTCP nanoparticles at the excitation wavelength of 325 nm are shown in Fig. 2. At this excitation wavelength, the best and maximum fluorescence intensity of ZnO and ZnO-Cys nanoparticles was recorded around 400 nm, which is placed in the blue part of the visible spectrum because of the stimulating wide band gap of ZnO in 3.37 eV [29]. Thus, the obtained ZnO nanoparticles were highly pure and existed as a crystalline form [28]. There is no compulsory overlap between the absorption and excitation spectra because absorption spectrum is dependent on all possible electronic transitions in the structure of a matter, whereas excitation spectrum is associated with those electronic transitions having the potential to emit fluorescence photons. Thus, it is natural if the best excitation of ZnO-Cys can be achieved at 325 nm, which is 75 nm above the maximum absorbance at 250 nm (Fig. 2).

The fluorescence intensity of the ZnO-Cys nanoparticles increases with decreasing particle size [30]. This was attributed to the increased surface area of the nanoparticles relative to their volume, when the particle size was decreased. Decreasing the size is followed by exposure of the electron trap layers on the surface of the particles, resulting in the increased fluorescence intensity of the nonaggregated and diminutive nanoparticles [30]. Thus, absorption and emission peak of ZnO-Cys nanoparticles were stronger than ZnO nanoparticles. The cysteine coating of the nanoparticles prevented their aggregation, decreased their size, and increased their fluorescence intensity after excitation.

Fluorescence spectra of the porphyrin-conjugated nanoparticles demonstrated that the fluorescence intensity of ZnO-Cys nanoparticles was largely quenched around 370 nm after

conjugation with MTCP or CuMTCP (Fig. 2). This was attributed to FRET between the cysteine-coated ZnO nanoparticles and the conjugated porphyrin moieties and provides strong evidence for the successful conjugation process. The remained fluorescence intensity around 370 nm was related to the residual photons of ZnO-Cys, which was not absorbed by the bound porphyrins. The newly exhibited fluorescence peak at the vicinity of 470 nm related to the FRET between ZnO-Cys and the porphyrins (Fig. 2). The intensity of this newly exhibited peak (scaled at the right axis) is significantly lower than that of ZnO-Cys showing effective absorption of the emitted photons by the molecular oxygen to produce superoxide anion or free radicals. Absorption spectra of MTCP and CuMTCP effectively overlapped with fluorescence spectra of ZnO nanoparticles as shown in Fig. 3. Therefore, with respect to the FRET between ZnO-Cys and MTCP or CuMTCP, these porphyrin moieties can be activated to work as photosensitizers and produce ROS in the medium. ROS is a general term that characterizes $O_2$-derived free radicals such as hydroxyl radicals ($OH^{\bullet}$) superoxide anions ($O_2^{\bullet}$), peroxyl ($RO_2^{\bullet}$), alkoxyl ($RO^{\bullet}$), and nonradical species such as $H_2O_2$ and singlet oxygen ($O_2^{*}$). The major intracellular source of ROS is mitochondrion [31]. Among the ROS-generating systems in mitochondrion, $\alpha$-ketoglutarate dehydrogenase and pyruvate dehydrogenase are significantly involved in $O_2^{\bullet}$ and $H_2O_2$ production [32]. Another source of cellular $H_2O_2$ is peroxisomes. Endoplasmic reticulum also contributes to the production of cellular $H_2O_2$ and $O_2^{\bullet}$ via cytochrome P450 activity. ROS promotes lipid peroxidation, mitochondrial dysfunction, and cell apoptosis [33, 34]. ROS may be responsible for the decrease in Bcl-xL mRNA levels that precede the loss of $\Delta\psi_m$, the release of cytochrome *c*, and the activation of caspase-3, augmenting cell death [35–37]. There are several cellular redox systems such as glutathione, thioredoxin, peroxyredoxins (Prx), pyridine nucleotides (NADH/NADPH), and some polysaccharides maintain an optimal intracellular redox environment for free radical scavenging and inhibition of apoptosis [38].

In SLPDT, the main goal is to excite the first photoresponder (ZnO) to emit photons toward the main photosensitizer (porphyrin) until the excitation of the main photosensitizer can occur effectively for ROS production and cell killing. The excitation of the first photoresponder may occur at an inadequate wavelength, such as the UV range, with no good tissue penetration. However, the effective relaying of the emission photons from the nanoparticle core towards the photosensitizer, placed on the surface of the nanoparticle–photosensitizer conjugate, results in a stronger activation of photosensitizer than the state in which activation of the photosensitizer prepared via direct irradiation. Nonetheless, SLPDT under UV irradiation can be useful for the exposed and accessible cancers such as skin cancers in which penetration of 1 mm of UV can be utilized for therapy. For treatment of deep cancers via SLPDT, X-ray activation of the nanoparticle moiety can be substituted to excite the conjugated porphyrin to overcome the problem of low tissue penetration of the UV light (see below). This type of SLPDT was previously suggested by Chen and Zhang, although they did not reported any experimental data to prove the potency of their suggestion for cell killing [1]. A coordinated form of $Cu^{2+}$ exists in the center of the porphyrin ring of CuMTCP. However, the free atomic orbital's of $Cu^{2+}$ might be coordinated with the ROS including singlet oxygen produced under UV irradiation [39]. This also occurs in hemoglobin when the two coordination numbers of the iron ion are consumed by His

residue and $O_2$ binding [40]. Thus, under these conditions the effective concentration of ROS not only will decrease in the medium but also reduce the emission characteristics of CuMTCP in its free or conjugated form. The lower potency of CuMTCP was also supported by the cytotoxicity tests when the T-47D and Du145 cells were incubated with CuMTCP and ZnO-CuMTCP (discussed below).

The attachment of MTCP to ZnO nanoparticles was further confirmed by FTIR spectroscopy. FTIR spectra of ZnO and ZnO-MTCP are shown in Fig. 4. The peaks around 3,000 $cm^{-1}$ were attributed to the stretching vibration of the N–H group in MTCP. In ZnO-MTCP, the strong peak around 1,380 $cm^{-1}$ was arisen from vibration of the amide bond. Spectra of 965 and 870 $cm^{-1}$ were related to C–C and C–H bonds [41]. These results indicated that MTCP was bound to cysteine-coated ZnO nanoparticles via the amide bonds since the peak of the –NH group around 3,000 $cm^{-1}$ was eliminated and instead a peak for the amide bond was appeared at 1,380 $cm^{-1}$.

We next incubated the generated nanoparticles with cells in culture. Nearly 5 H after the addition of free MTCP, ZnO or ZnO-MTCP nanoparticles to cultures of T-47D and Du145, cell their uptake was determined using a fluorescence microscope (Figs. 5b–5d and 6b–6d). On the whole, the uptake and accumulation of the materials in the T-47D cells occurred much better compared with Du145 cells. This was attributed to the resistance of Du145 cells against the uptake of the nanoparticles and their protection from the nanoparticle-induced cell death (see below). There are a few reports discussing cellular excretion and degradation of nanoparticles. They all conclude that the exocytosis of nanoparticles is much slower than their endocytosis, which decreases with increasing particle size [42, 43]. The rate of exocytosis is different in different cell lines, but it occurs approximately 1 H after endocytosis [42]. The stability of various nanoparticles differs after cellular uptake. Some studies have also focused on the possible cellular metabolism of biodegradable nanoparticles including polylactic acid polymers, liposomes, and metal-based nanoparticles [44–46].

To prepare microscopic images, the treated cells were first fixed with paraformaldehyde. The paraformaldehyde reacts with the proteins and free amino groups, especially in the cell membrane, making it autofluorescence, which interferes with photoluminescence of the nanoparticles accumulated in the cells. The autofluorescence of the cells was eliminated by incubating the cells with sodium borohydrate (Figs. 5a and 6a). Enhanced green luminescence of the cells after treatment with cysteine-coated ZnO nanoparticles is shown in Figs. 5b and 6b. The optical settings in our fluorescence microscopy provided an adequate condition for simultaneous imaging of red and green fluorescence. The excitation band pass filter in our microscopic studies caused the UV-A to pass through and absorb by ZnO-Cys nanoparticles, resulting in green fluorescence (Figs. 5b and 6b). The green fluorescence could be absorbed by conjugated MTCP and produce the new fluorescence at higher wavelength (around 470 nm as shown in Fig. 2). The redshift of the final fluorescence is a basic concept in FRET phenomena. The cellular entrance of MTCP-conjugated form of cysteine-coated ZnO nanoparticles is shown in Figs. 5c and 6c. In these figures, the green fluorescence of ZnO-Cys in Figs. 5b and 6b was shifted toward the green-yellow fluorescence with a higher wavelength, proving the successful FRET between conjugated MTCP and ZnO-Cys nanoparticles, which was further supported by FTIR (Fig. 4). A

decrease in the total green-yellow fluorescence in Figs. 5c and 6c (relative to the pure green fluorescence in Figs. 5b and 6b) occurred because the emitted photons were partially absorbed by the molecular oxygen to produce superoxide anions, as shown in Fig. 2. The natural red fluorescence of free unconjugated MTCP can be observed with UV exposure of the exciting photons supplied directly by the microscope light source (Figs. 5d and 6d). However, when MTCP is conjugated with ZnO nanoparticles then the main supplier for exciting photons (having different wavelength from the microscope light source) is ZnO nanoparticles, producing green-yellow emission photons from conjugated MTCP instead of the red one coming from its free form (Figs. 5c and 6c).

Cytotoxic effects on the two selected cell lines (T-47D and Du145) were determined for different concentrations of nanoparticles in the dark or after UV or X-ray irradiation by MTT assays, and the results are shown in Fig. 7. Cells were incubated with ZnO, ZnO-MTCP, and ZnO-CuMTCP nanoparticles at 10 (black column), 30 (dark gray column), and 60 μM (gray column). Cells were also incubated with free MTCP and CuMTCP at 0.75 (black column), 1.5 (dark gray column), and 7.5 μM (gray column). The concentrations greater than 7.5 μM showed considerable cytotoxic effects with or without UV or X-ray irradiation, and the concentrations below 0.75 μM did not show any significant cytotoxicity even under UV or X-ray irradiation (not shown). Thus, we selected the middle concentration (1.5 μM) for our cell treatments. This concentration was in the range of previously reported concentration for ZnO-bound porphyrin that was utilized in another study using meso-tetra *o*-amino phenyl porphyrin (MTAP).

With respect to the reported bioconjugation method of ZnO nanoparticles (using the porphyrins), the molar concentration of the synthesized porphyrin-conjugated ZnO nanoparticles after the conjugation reaction was 5 mM [16, 17]. Regarding the cytotoxic effects of ZnO-MTAP, Liu et al. were forced to dilute the product of the bioconjugation reaction up to 30 μM for MTT assessments. We also carried out MTT investigations using 30 μM of ZnO-MTCP or ZnO-CuMTCP nanosystem. Furthermore, two additional concentrations of ZnO-porphyrin nanosystems (60 and 10 μM) were also studied to obtain more accurate results.

Liu et al. reported that the molar concentration of the ZnO-bound MTAP was a quarter of the molar concentration of ZnO nanoparticle (7.5 μM that is one fourth of 30 μM ZnO). Therefore, we also focused on the same concentration to carry out MTT assessments for the free MTCP and CuMTCP. Here, cytotoxic effects of two further concentrations of MTCP and CuMTCP (1.5 and 0.75 μM) were also investigated. It should be noted that the cytotoxic effects of the free porphyrins at high concentrations (e.g., 15 μM, which is one fourth of 60 μM ZnO-porphyrin nanosystems) could not be studied because at these concentrations the unwanted cytotoxic effects of the free MTCP and CuMTCP were exhibited even in the dark. Based on the PDT principles, it is preferred that none of the constructing ingredients of a photodynamic system exhibit individual cytotoxicity, whether in the dark or under irradiation.

The percent viability of T-47D and Du145 cells incubated with ZnO, ZnO-MTCP, and ZnO-CuMTCP nanoparticles (10, 30, and 60 μM) in the dark is shown in Fig. 7A. Similar results

are also indicated for free MTCP and CuMTCP (0.75, 1.5, and 7.5 μM) in Fig. 7B. These results showed that none of the free porphyrins or free ZnO exhibit cytotoxic effects in the dark ($P > 0.05$) (Figs. 7A and 7B). This also occurred for ZnO-MTCP and ZnO-CuMTCP when they were incubated with T-47D and Du145 cells in the dark.

Under UV irradiation, the MTT results showed that incubation of T-47D and Du145 cells with ZnO, ZnO-MTCP, and ZnO-CuMTCP nanoparticles resulted in significant cytotoxic effects, especially at the highest concentration (60 μM), demonstrating the sensitive nature of these cells to PDT (Fig. 7C). We used a safe condition for the time and intensity of UV irradiation, which by themselves lacked cytotoxicity (not shown). This was performed since in PDT the two factors, namely chemical matter (ZnO-porphyrins) and radiation (UV-A/B), both used under their safe conditions, but their synergistic effects causes cytotoxicity to be more effective than their individual use. The free MTCP and CuMTCP did not exhibit any significant cytotoxic effects under UV irradiation (Fig. 7D). However, when they were conjugated to ZnO nanoparticles, effective FRET between ZnO and the conjugated porphyrins was occurred causing better free radical production with more cytotoxic effects compared to ZnO alone. The FRET between ZnO and conjugated MTCP or CuMTCP was also confirmed by fluorescence spectrophotometry (Fig. 2). Among the unconjugated forms of the used materials, free ZnO was the only unique material showing cytotoxic effects with UV irradiation, especially at the highest concentration (60 μM) in Du145 cells (Fig. 7C). So, unlike the free porphyrins, free ZnO could produce ROS individually. Thus, the cytotoxic effects of ZnO-MTCP and ZnO-CuMTCP under UV irradiation were partly related to the ZnO and partly to the porphyrin moiety excited via FRET.

The low cytotoxic effects exhibited by ZnO-CuMTCP (especially in Du145 cells) showed that killing potency for this conjugated nanoparticle was much lower than that of ZnO-MTCP (Fig. 7C). In T-47D cells, the lethal effects were exhibited at the three concentrations of ZnO-CuMTCP (10, 30, and 60 μM) under UV irradiation, but these were lower than that of ZnO-MTCP and were completely absent, even at the highest concentration in Du145 cells (Fig. 7C). On the other hand, cytotoxic effects of free ZnO as well as ZnO-MTCP were exhibited at the three concentrations of 10, 30, and 60 μM in T-47D cells, but these were only seen at the highest concentration (60 mM) in Du145 cells (Fig. 7C). Collectively, these results demonstrated the more resistant nature of Du145 cells, perhaps as a result of a special defense mechanism against the uptake of the nanoparticles into the cells. Our fluorescence microscopic results could verify this notion as described above (Figs. 6a–6d).

According to the MTT results, ZnO nanoparticles alone exhibited significant lethal effects on either T-47D or Du145 cell lines under X-ray illumination (Fig. 7E). This notion was especially exhibited at 60 μM even more effectively than the cytotoxicity of ZnO-porphyrin conjugates under UV irradiation. Treatment of both cell lines with ZnO-MTCP and ZnO-CuMTCP did not show any cytotoxic effects on the cells as well as for free MTCP or CuMTCP (Fig. 7F). So this was unlike the previous suggestion propounded by Chen and Zhang [1]. This inconsistency might be due to the failed FRET between ZnO and the conjugated porphyrins that is necessary for the effective ROS production and cell killing.

## 4. Conclusions

ZnO-based nanosystems can be stimulated by UV or X-ray irradiation leading to death of cancer cells. Here, ZnO nanoparticles were developed and linked covalently with photoactive porphyrin molecules MTCP or CuMTCP, which are able to highly absorb the emission photons irradiated from the cysteine-coated nanoparticles and establishing a SLPDT nanosystem. Collectively, our results support the successful attempt to synthesize ZnO-porphyrin nanosystems. However, the efficient FRET between ZnO and porphyrin for cell killing was only exhibited under UV irradiation. Under X-ray irradiation, cells were not killed possibly due to lack of FRET between ZnO moiety and the conjugated porphyrins. However, ZnO nanoparticles alone could result in significant cell killing under X-ray irradiation. The ZnO-MTCP conjugate entered the cells (especially T-47D cells) and decreased the survival of two selected cell lines (especially at the highest concentration) when irradiated with a safe intensity UV light. This notion was partially true for ZnO-CuMTCP because in T-47D cells cellular effects were exhibited only at the highest concentration. No cellular effects were displayed in Du145 cells because of a cellular mechanism preventing the uptake of ZnO-CuMTCP. Thus, it appears that ZnO-MTCP nanoparticles provide a suitable nanochemical system with sufficient potency as a drug, at least for treatment of the exposed cancers using UV irradiation. Furthermore, ZnO acted alone as a potent cytotoxic nanoparticle under X-ray irradiation making it useful for treatment of deep cancers.

## Acknowledgments

The support of the Iran National Science Foundation (INSF) is gratefully appreciated. The authors would also like to thank the Iran Nanotechnology Initiative Council and Research Council of University of Tehran for their patronage. The authors have no conflict of interest.

## Abbreviations

| | |
|---|---|
| **DMSO** | dimethyl sulfoxide |
| **EDC** | 1-ethyl-3-(3-dimethyl aminopropyl)carbodiimide |
| **eV** | electron volt |
| **FBS** | fetal bovine serum |
| **FRET** | fluorescence resonance energy transfer |
| **FTIR** | fourier transform infrared |
| **kV** | kilovolt |
| **MTCP** | (meso-tetra(4-carboxyphenyl) porphyrin |
| **MTT** | 3-[4, 5-dimethylthiazol-2-yl]-2,5-diphenyl tetrazolium bromide |
| **PBS** | phosphate buffer saline |
| **PDT** | photodynamic therapy |

| | |
|---|---|
| **ROS** | reactive oxygen species |
| **RPMI** | Roswell Park Memorial Institute |
| **SLPDT** | self-lighting photodynamic therapy |
| **sulfo-NHS** | N-hydroxysulfosuccinimide |
| **TEM** | transmission electron microscopy |
| **UV-vis** | ultraviolet-visible |

## References


1. Chen W, Zhang J. Nanosci Nanotechnol. 2006; 6:1159–1166.
2. Nie S, Xing Y, Kim GJ, Simons JW. Annu Rev Biomed Eng. 2007; 9:257–288. [PubMed: 17439359]
3. Kingsley JD, Dou H, Morehead J, Rabinow B, Gendelman HE, Destache CJ. J Neuroimmune Pharmacol. 2006; 1(3):340–350. [PubMed: 18040810]
4. Kairemo K, Erba P, Bergström K, Pauwels KJ. Curr Radiopharm. 2009; 1:30–36.
5. Rhyner MN, Smith AM, Gao X, Mao H, Yang L, Nie S. Nanomedicine (Lond). 2007; 1:209–217.
6. Li M, Bala H, Lv X, Ma X, Sun F, Tang L, Wang Z. Phys Chem B. 2007; 61:690–693.
7. Hanley C, Thurber A, Hanna C, Punnoose A. Nanoscale Res Lett. 2009; 4:1409–1420. [PubMed: 20652105]
8. Moos PJ, Chung K, Woessner D, Honeggar M, Cutler NS, Veranth JM. Chem Res Toxicol. 2010; 23:733–739. [PubMed: 20155942]
9. Akhtar MJ, Ahamed M, Kumar S, Khan MM, Ahmad J, Alrokayan SA. Int J Nanomedicine. 2012; 7:845–857. [PubMed: 22393286]
10. Setyawati MI, Tay CY, Leong DT. Biomaterials. 2013; 34:10133–10142. [PubMed: 24090840]
11. Tay CY, Setyawati MI, Xie J, Parak WJ, Leong DT. Adv Funct Mater. 2014; 24:5936–5955.
12. Setyawati MI, Tay CY, Chia SL, Goh SL, Fang W, Neo MJ, Chong HC, Tan SM, Loo SC, Ng KW, Xie JP, Ong CN, Tan NS, Leong DT. 2013; 4:1673.
13. Zhao Y, Howe JLC, Yu Z, Leong DT, Chu JJH, Loo JSC, Ng KW. Small. 2013; 9:387–392. [PubMed: 23090781]
14. Alarifi S, Ali D, Alkahtani S, Verma A, Ahamed M, Ahmed M, Alhadlaq HA. Int J Nanomed. 2013; 8:983–993.
15. Bechet D, Couleaud P, Frochot C, Viriot ML. Trends Biotechnol. 2008; 26:612–21. [PubMed: 18804298]
16. Liu Y, Chen W, Wang S, Joly AG. Appl Phys Lett. 2008; 92:043901.
17. Liu Y, Zhang Y, Wang S, Pope C, Chen W. Appl Phys Lett. 2008; 92:143901.
18. Li J, Guo D, Wang X, Wang H, Jiang H, Chen B. Nanoscale Res Lett. 2010; 5:1063–1071. [PubMed: 20671778]
19. Rasmussen JW, Martinez E, Louka P, Wingett DG. Expert Opin Drug Deliv. 2010; 7:1063–1077. [PubMed: 20716019]
20. Akhtar MJ, Ahamed M, Kumar S, Khan M, Ahmad J, Alrokayan SA. Int J Nanomed. 2012; 7:845–857.
21. Reddy KM, Feris K, Bell J, Wingett DG, Hanley C, Punnoose A. Appl Phys Lett. 2007; 24:2139021.
22. Cheng HM, Hsu HC, Chen SL, Wu WT, Kao CC, Lin L, Hsieh WF. J Cryst Growth. 2005; 277:192–199.
23. Mosmann T. J Immunol Methods. 1983; 65:55–63. [PubMed: 6606682]
24. Nair S, Sasidharan A, Rani VD, Menon D, Nair S, Manzoor K, Raina. J Mater Sci, Mater Med. 2009; 1:S235–S241.

25. Shen L, Bao N, Yanagisawa K, Domen K, Gupta A, Grimes CA. Nanotechnology. 2006; 17:5117–5123.
26. Hermans, GT. Bioconjugate Techniques. Academic Press; New York: 1996.
27. Bhat SV, Vivekchand SRC, Govindaraj A, Rao CNR. Solid State Commun. 2009; 149:510–514.
28. Shah MA. Afr Phys Rev. 2008:2106–2109.
29. Chen CS, Chen XH, Yi B, Liu TG, Li WH, Xu LS, Yang Z, Zhang H, Wang YG. Acta Mater. 2006; 54:5401–5407.
30. Wang Z, Zhang H, Zhang L, Yuan J, Yan V, Wang V. Nanotechnology. 2003; 14:11–15.
31. Halliwell B, Cross CE. Environ Health Perspect. 1994; 102:5–12.
32. Starkov AA, Fiskum G, Chinopoulos C, Lorenzo BJ, Browne SE, Patel MS, Beal MF. J Neurosci. 2004; 24:7779–7788. [PubMed: 15356189]
33. Zangar RC, Davydov DR, Verma S. Toxicol Appl Pharmacol. 2004; 199:316–33115. [PubMed: 15364547]
34. Caro AA, Cederbaum AI. Free Radic Biol Med. 2006; 40:364–375. [PubMed: 16443151]
35. Herrera B, Alvarez AM, Sánchez A, Fernández M, Roncero C, Benito M, Fabregat I. FASEB J. 2001; 15:741–751. [PubMed: 11259392]
36. Tang W, Liu JW, Zhao WM, Wei DZ, Zhong JJ. Life Sci. 2006; 80:205–211. [PubMed: 17007887]
37. Liu RM, Li Y Bo, Zhong JJ. Lat Am J Pharm. 2012; 31:43–50.
38. Xiao JH, Xiao DM, Chen DX, Xiao Y, Liang ZQ, Zhong JJ. Evid Based Complement Alternat Med. 2012; 2012:273435. [PubMed: 22536281]
39. DeRosa MC, Crutchley RJ. Coord Chem Rev. 2002; 233–234:351–371.
40. Nelson, DL.; Cox, MM. In Principle of Biochemistry. W. H. Freeman; New York: 2008. p. 154-158.
41. Coates, J.; Meyers, RA. In Encyclopedia of Analytical Chemistry. Wiley; Hoboken, NJ: 2000. p. 10815-10837.
42. Chithrani BD, Chan WC. Nano Lett. 2007; 7:1542–1550. [PubMed: 17465586]
43. Jin H, Heller DA, Sharma R, Strano MS. ACS Nano. 2009; 3:149–158. [PubMed: 19206261]
44. Torchilin VP. Adv Drug Deliv Rev. 2006; 58:1532–1555. [PubMed: 17092599]
45. Igarashi E. Toxicol Appl Pharmacol. 2008; 229:121–134. [PubMed: 18355886]
46. Iversena TG, Skotlanda T, Sandviga K. Nano Today. 2011; 6:176–185.

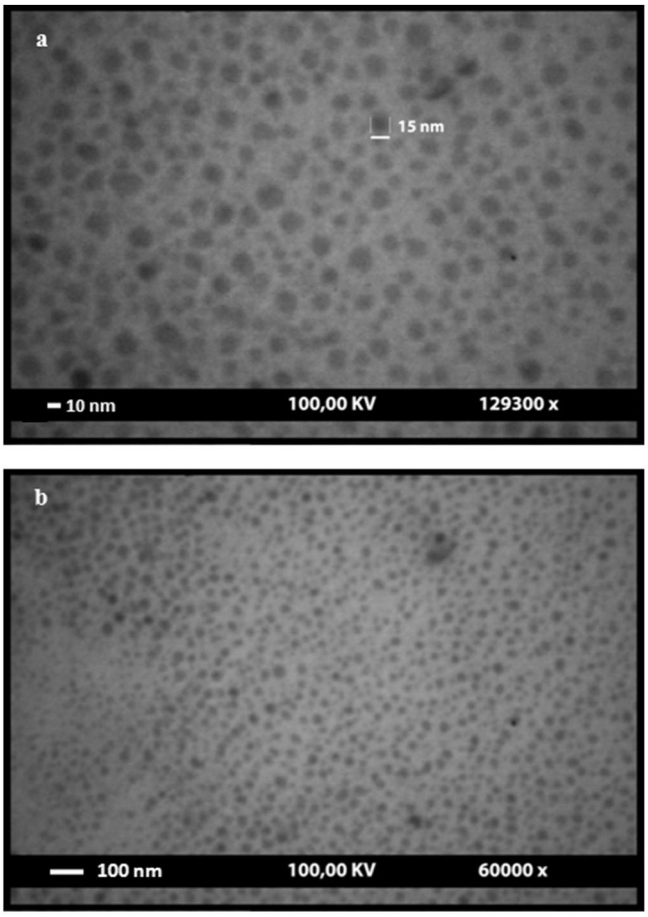


**FIG. 1.**

Transmission electron microscopic images of ZnO nanoparticles coated with cysteine. These images present spherical and hexagonal structures of the ZnO nanoparticles with the approximate size of 3–26 nm. (a) 129,300× and (b) 60,000× magnification.

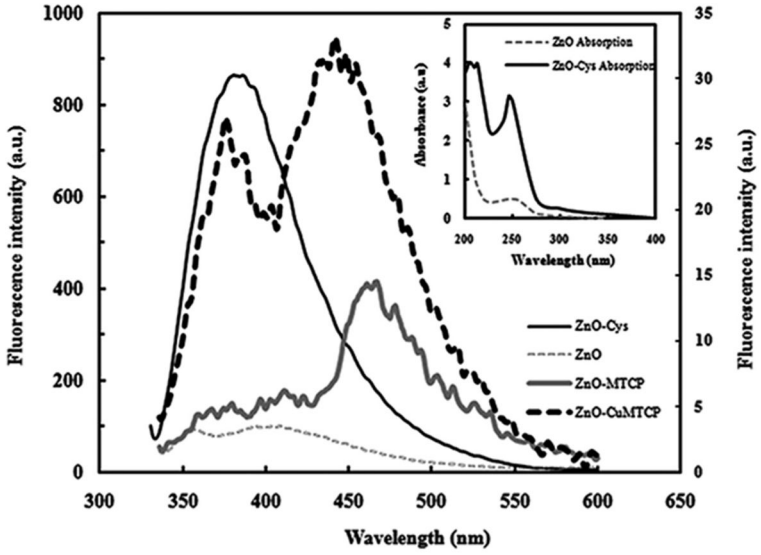


**FIG. 2.**

Fluorescence spectra of uncoated ZnO, ZnO-Cys, ZnO-MTCP, and ZnO-CuMTCP nanoparticles. Quenching of the fluorescence spectrum of ZnO-Cys around 370 nm showed that when it was conjugated to MTCP or CuMTCP, then an attachment between porphyrins and ZnO-Cys nanoparticles should be effectively occurred to show FRET phenomenon. Conjugation of the porphyrins produced additional bands in the vicinity of 470 nm. This was mainly attributed to the fine quality of the synthesized ZnO-porphyrin. The fluorescence intensity of ZnO-MTCP and ZnO-CuMTCP are shown on the right-hand side of the secondary axis since they were much lower than that of ZnO and ZnO-Cys (a.u. denotes arbitrary units). Excitation wavelength was 325 nm. Inset: Absorption spectra of ZnO and ZnO-Cys nanoparticles. Absorbance of ZnO-Cys nanoparticles was increased, indicating smaller size of nanoparticles acting as a better quantum dot. (a.u. denotes absorbance units).

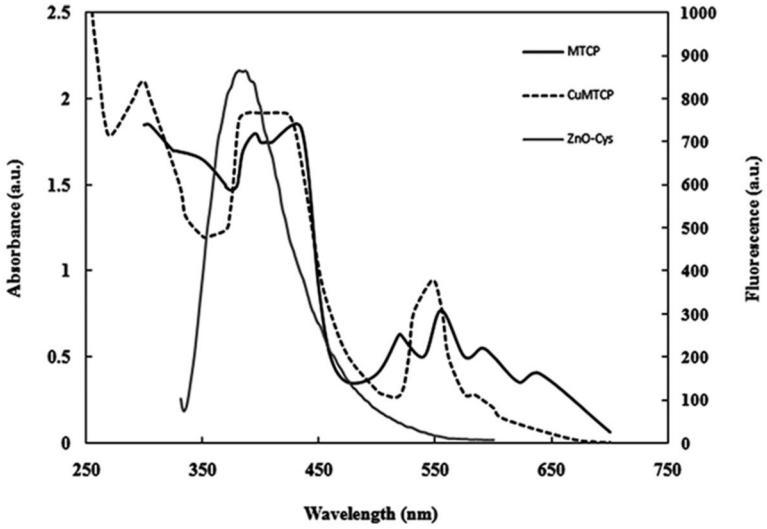


**FIG. 3.**

Comparison of fluorescence spectra of ZnO-Cys (scaled at the right-hand side of secondary axis) with the absorption spectra of MTCP and CuMTCP scaled at the left-hand side of the primary axis. The overlapped absorption spectra of MTCP or CuMTCP with the fluorescence spectrum of ZnO-Cys indicated the successful occurrence of the FRET. The a.u. denotes absorbance units (left axis) or arbitrary units (right axis).

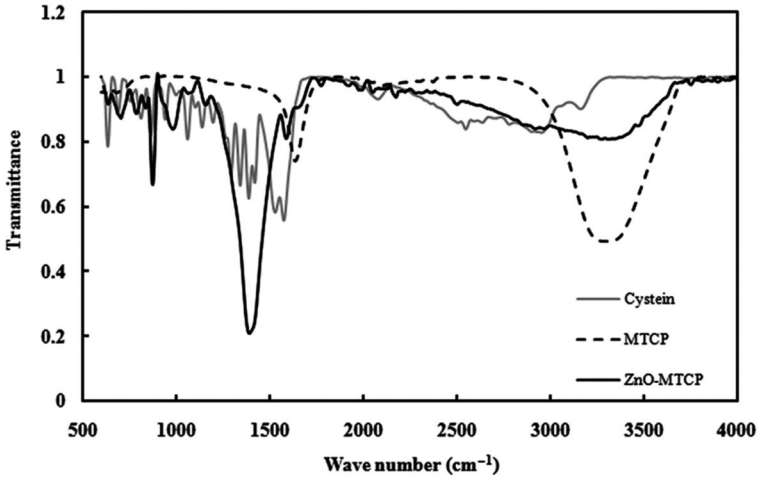


**FIG. 4.**

FTIR spectra of ZnO-MTCP, cysteine, and MTCP. The peaks around 3,000 $cm^{-1}$ are attributed to the stretching vibration of the N–H group present in MTCP. The strong peak around 1,380 $cm^{-1}$ aroused from vibration of the amide bond. Elimination of the peak around 3,000 $cm^{-1}$, and exhibition of strong peak around 1,380 $cm^{-1}$, demonstrates the formation of the amide bond between MTCP and the cysteine arm on ZnO nanoparticles.

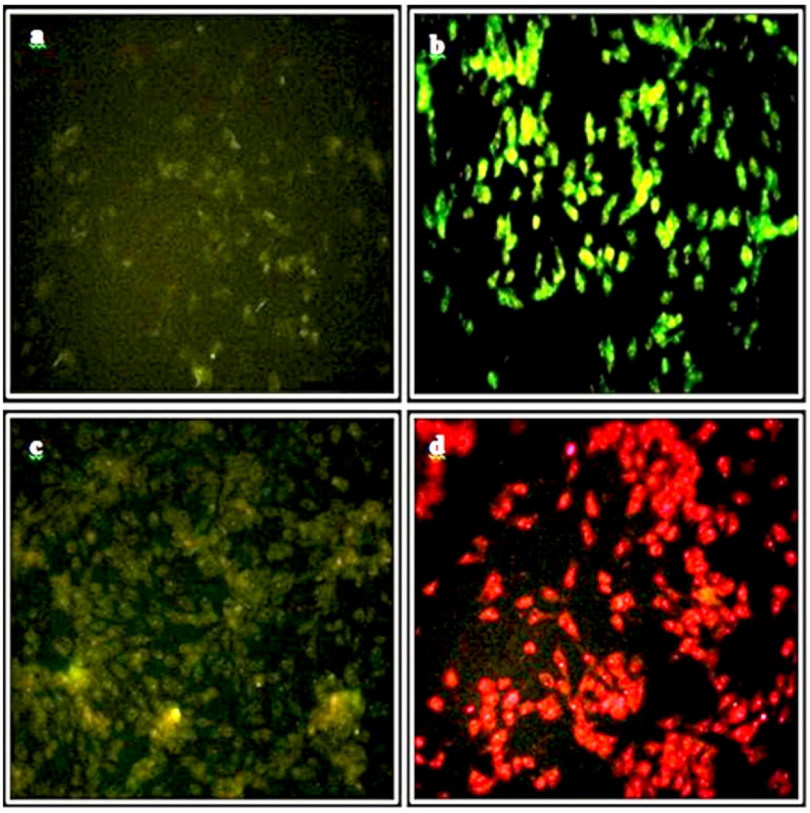


**FIG. 5.**

Fluorescence microscopic analysis of T-47D cells incubated with ZnO, ZnO-MTCP or free MTCP. (a) No background green emission of the control cells. (b) Green emission of the cells incubated with 60 μM zinc oxide nanoparticles coated with cysteine (ZnO-Cys). (c) Green-yellow emission of the cells incubated with 60 μM of cysteine-coated ZnO nanoparticles conjugated with MTCP (ZnO-MTCP). Fluorescence was partially reduced relative to (b) because of effective absorption of the green-yellow emitted photons by the molecular oxygen producing superoxide anions or free radicals. The entrance of ZnO-porphyrin (c) was higher than ZnO-Cys (b) supporting the increased tendency of ZnO-porphyrin for entering the cells. (d) Intrinsic red fluorescence of free and unconjugated MTCP (1.5 μM) trapped in the cells. Magnification was 250×.

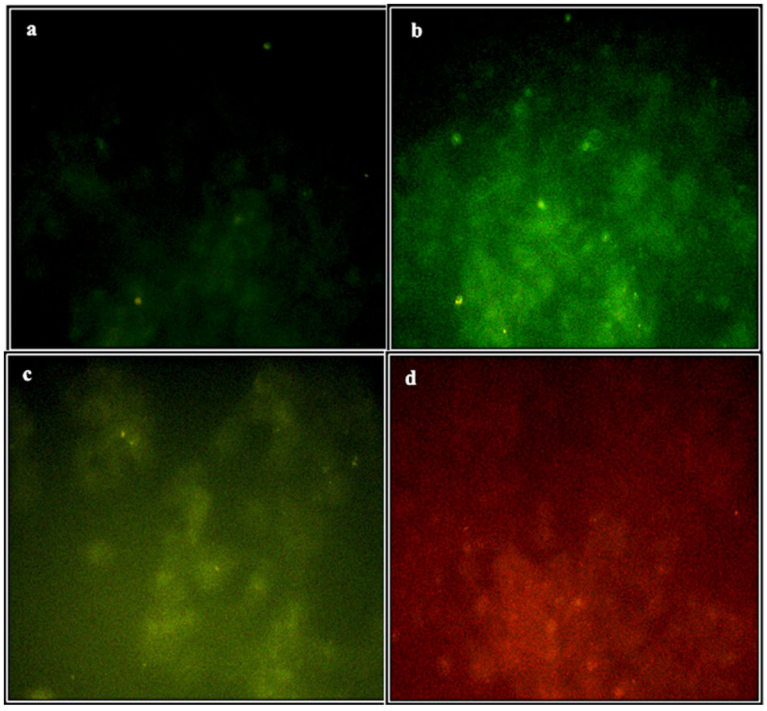


**FIG. 6.**

Fluorescence microscopy analysis of Du145 cells incubated with ZnO-Cys, ZnO-MTCP, or free MTCP. (a) No background green emission of the control cells. (b) Green emission of the cells incubated with 60 μM zinc oxide nanoparticles coated with cysteine (ZnO-Cys). There was no significant uptake and accumulation of the nanoparticles in Du145 cells compared with T-47D cells (Fig. 5). (c) Green-yellow emission of the cells incubated with 60 μM of cysteine-coated ZnO nanoparticles conjugated with MTCP (ZnO-MTCP). (d) Intrinsic red fluorescence of free and unconjugated MTCP (1.5 μM) trapped partially in the cells. Magnification was 250×.

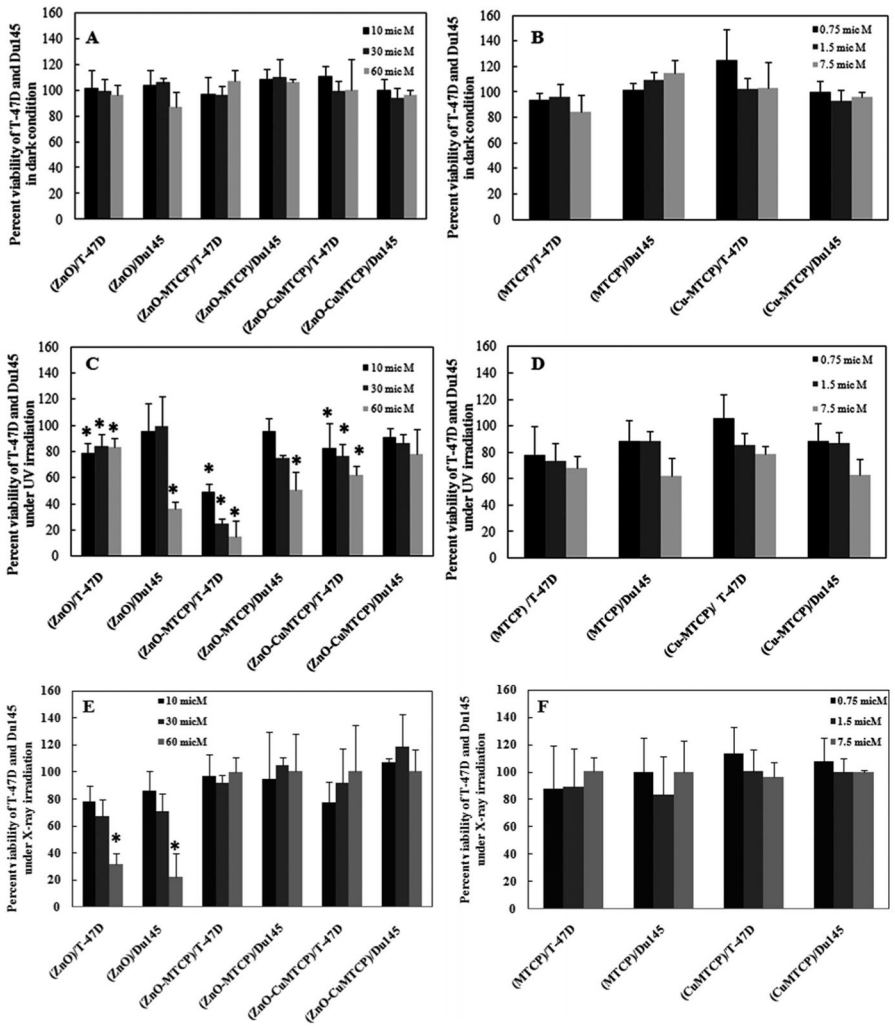


**FIG. 7.**

Column histograms of the cytotoxic effects of ZnO, ZnO-porphyrins, MTCP, and CuMTCP in T-47D and Du145 cells in the dark, and under UV or X-ray irradiations. Cytotoxicity was assessed using MTT assay in the presence of ZnO, ZnO—porphyrins, and free porphyrins (MTCP and CuMTCP). Untreated T-47D and Du145 cells (no drug treatment and no irradiation) were used as the control in (A) and (B) exhibiting 100% viability. The used controls in (C)–(F) were drug-treated cells receiving irradiation. (A) Each set of data (triple columns) relates to the three different concentrations of ZnO-based nanoparticles (10 μM, black column; 30 μM, dark gray; 60 μM, gray) in the dark condition. (B) Concentrations of the free porphyrins (MTCP or CuMTCP) were 0.75 μM, black column; 1.5 μM, dark gray; and 7.5 μM, gray in dark condition. The concentration of the porphyrins, when they were bound to the nanoparticles, was 1.5 μM. (C) Percent viability of T-47D and Du145 cells incubated with ZnO, ZnO-MTCP, and ZnO-CuMTCP (10, 30, and 60 μM) under UV irradiation. (D) The free porphyrins (MTCP or CuMTCP) effects on T-47D and Du145 cells in concentrations of 0.75, 1.5, and 7.5 μM under UV irradiation. (E) Percent viability of T-47D and Du145 cells incubated with ZnO, ZnO-MTCP. and ZnO-CuMTCP (10, 30, and

60 μM) under X-ray irradiation (0.94 Gy for 30 Sec). (F) The free porphyrin effects (MTCP or CuMTCP) on T-47D and Du145 cells were studied in concentrations of 0.75, 1.5, and 7.5 μM under X-ray irradiation. Statistical analysis was performed between dark or UV and also dark and X-ray states for at least three separate experiments. The time and intensity of UV or X-ray irradiation in our studies was adjusted using several assessments to obtain an adequate condition in which no cytotoxic effects were seen for UV or X-ray alone. Thus, toxicity of UV and X-ray were negligible by themselves and it is eliminated in the presentation of data. $P < 0.05$ means statistically significant between two states of dark and UV or X-ray and is indicated with the * symbol.

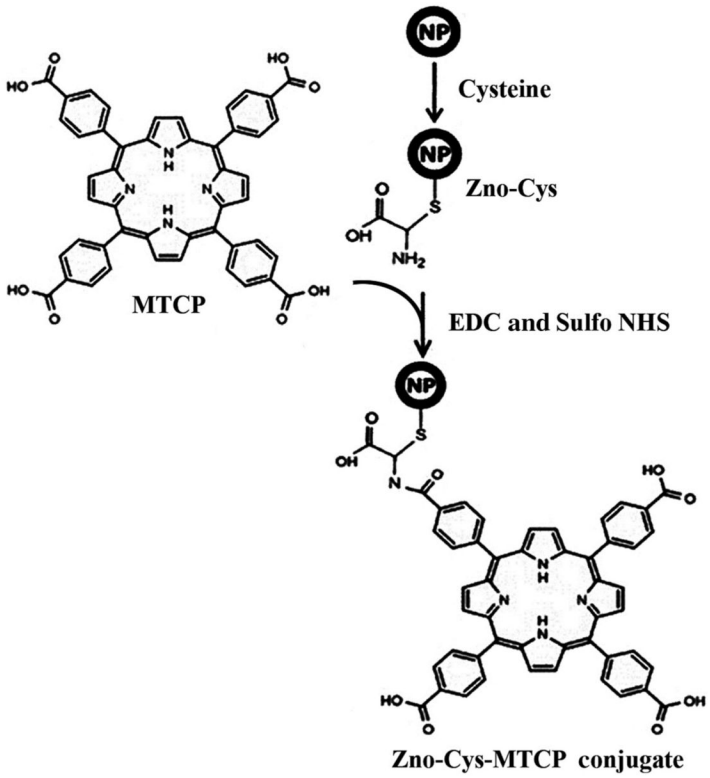


**Scheme 1.**

Schematic representation of the reaction of zinc oxide nanoparticle with cysteine. To avoid complexity, only one cysteine and its bound MTCP group are shown.